THE ASTROPHYSICAL JOURNAL, 538:L175–L178, 2000 August 1

A UNIFIED MODEL OF CORONAL MASS EJECTION–RELATED TYPE II RADIO BURSTS

TETSUYA MAGARA,[1] PENGFEI CHEN,[2] KAZUNARI SHIBATA,[3] AND TAKAAKI YOKOYAMA[4]

Received 2000 April 4; accepted 2000 June 16; published 2000 July 25

ABSTRACT

We present a theoretical model for the shock formation that is related to coronal and interplanetary type II radio bursts associated with coronal mass ejections on the basis of the magnetic reconnection model of eruptive solar flares. Coronal type II bursts are usually observed in the metric wavelength range (metric type II bursts), and interplanetary bursts are usually observed in the decametric-hectometric wavelength range (decametric-hectometric bursts). Our research shows that the decametric-hectometric type II radio bursts are produced by the piston-driven fast-mode MHD shock that is formed in front of an eruptive plasmoid (a magnetic island in the two-dimensional sense or a magnetic flux rope in the three-dimensional sense), while the metric radio bursts are produced by the reverse fast-mode MHD shock that is formed through the collision of a strong reconnection jet with the bottom of the plasmoid. This reverse shock apparently moves upward as long as the reconnection jet is sufficiently strong and dies away when the energy release of the reconnection stops or weakens significantly. On the other hand, the piston-driven fast shock continues to exist when the plasmoid moves upward. Our model succeeds in explaining the observational result that the piston-driven fast shock that produces decametric-hectometric type II bursts moves faster and survives longer than the other shock.

Subject headings: MHD — Sun: corona — Sun: magnetic fields — Sun: radio radiation

1. INTRODUCTION

Coronal mass ejections (CMEs) are one of the most prominent phenomena observed in the solar atmosphere. The spatial size of these events is very large, and their influence on interplanetary space is very strong. For example, when a large CME occurs on the Sun, a lump of plasmoid sometimes travels toward the Earth at several hundred kilometers per second and causes a severe magnetostorm.

CMEs are characterized not only by their largeness in size but also by the number of phenomena associated with them. In fact, many solar phenomena are believed to have a direct or indirect relationship to CMEs, such as solar flares, prominence eruptions, helmet streamers, high-speed solar winds, coronal and interplanetary traveling shock waves, and so on. These CME-related phenomena can be observed in various kinds of electromagnetic waves, making it possible for many researchers to do detailed studies on this subject (Gosling et al. 1976; Low, Munro, & Fisher 1982; Kahler et al. 1985; Priest 1988; Steele & Priest 1989; Forbes 1990; Gopalswamy & Kundu 1992; Feynman & Hundhausen 1994; Feynman & Martin 1995; Low 1996; Rust & Kumar 1996; Gibson & Low 1998; Hundhausen 1999; Klassen et al. 2000).

The CME-related phenomena we discuss here are coronal and interplanetary traveling shock waves. Observationally, these two kinds of shocks are recognized as coronal and interplanetary type II radio bursts because shocks accelerate plasma particles so that the particles emit radio waves whose frequency is above the so-called plasma frequency. The plasma frequency is proportional to the square root of the gas density so that the coronal type II bursts are observed in high frequency (small wavelength) compared with the interplanetary bursts. So far, it has been well established by analyzing kilometric type II radio sources that the interplanetary shock is formed in front of a traveling plasmoid through its piston-driven effect. However, the formation process of the coronal shock that produces type II radio bursts in the metric wavelength range is not yet fully understood. One idea is that this shock is also produced by a plasmoid traveling in the corona through the same piston-driven effect as in interplanetary space (Cliver et al. 1999), and another idea is that it is not produced by a plasmoid but rather by a solar flare associated with the CME (Reiner et al. 2000).

Recently, Reiner et al. (2000), by using data from the *Wind* spacecraft and the Culgoora radio spectrograph, provided an interesting result to these CME-related shocks that clearly shows two evolutionary lines of coronal and interplanetary type II radio bursts. One of these evolutionary lines implies that a long-lasting emission source travels in interplanetary space at high speed (1000 km s^{-1}). This evolutionary line coincides well with that of the leading edge of a white-light CME observed simultaneously from the *Solar and Heliospheric Observatory* Large Angle and Spectrometric Coronagraph. On the other hand, the second evolutionary line implies that there is another source traveling in the corona at a lower speed than the other one (400 km s^{-1}).

Prompted by their results, we in this Letter try to provide a theoretical explanation for the properties of the two kinds of shocks, one of which moves in interplanetary space at high speed, emitting long-lasting decametric-hectometric type II radio bursts, and the other that moves slowly in the corona, emitting short-lived metric type II radio bursts. We performed two-dimensional MHD numerical simulations based on the reconnection model of eruptive solar flares, called the CSHKP (Carmichael-Sturrock-Hirayama-Kopp-Pneuman) model (Carmichael 1964; Sturrock 1966; Hirayama 1974; Kopp & Pneuman 1976), to investigate the eruptive process of the plasmoid with special attention paid to the shock formation. The aim of this Letter is to unify the formation processes of the two kinds of shocks in the CME evolution. Section 2 gives the description

[1] Department of Physics, Montana State University, EPS 264B, P.O. Box 173840, Bozeman, MT 59717-3840; magara@solar.physics.montana.edu.
[2] Department of Astronomy, Nanjing University, 22 Hankou Lu, Nanjing, Jiangsu 210093, China.
[3] Kwasan Observatory, Faculty of Science, University fo Kyoto, Yamashina-ku, Kyoto 607-8471, Japan.
[4] Nobeyama Radio Observatory, Minamimaki, Minamisaku, Nagano 384-1305, Japan.

of our model. Our results and discussion are presented in §§ 3 and 4, respectively.

2. MODEL

The basic equations are two-dimensional nonlinear, time-dependent, resistive, and compressive MHD equations, which are solved by the multistep implicit scheme (Hu 1989). The details of this method can be found in Chen et al. (1999). The initial condition of the simulation is almost in equilibrium, similar to that in P. F. Chen & K. Shibata (2000, in preparation). The configuration of the magnetic field is that a magnetic island centered at $(x, y) = (0, h_0) = (0, 2)$ overlies three magnetic arcades (see the left panel in Fig. 1). Here x and y define the horizontal and vertical coordinates, respectively. The flux function of the magnetic field is given by

$$\Psi = \begin{cases} \dfrac{B_0 r_0}{2}\left(\dfrac{r}{r_0}\right)^2 + f(x, y), & r \le r_0, \\ \dfrac{B_0 r_0}{2}\left[\ln\left(\dfrac{r}{r_0}\right)^2 + 1\right] + f(x, y), & r > r_0, \end{cases}$$

where $r \equiv [x^2 + (y - h_0)^2]^{1/2}$ and

$$f(x, y) = \Psi_0 \ln\left\{\frac{[(x + x_1)^2 + (y + y_1)^2][(x - x_1)^2 + (y + y_1)^2]}{[(x + x_2)^2 + (y + y_1)^2][(x - x_2)^2 + (y + y_1)^2]}\right\} - \frac{B_0 r_0}{2}\ln[x^2 + (y + h_0)^2].$$

In the present simulation, we adopt $B_0 = 1$, $\Psi_0 = 3.44$, $r_0 = 0.5$, $x_1 = 0.2$, $x_2 = 0.05$, and $y_1 = 0.05$ so that we make the center of the magnetic island remain stable for a sufficiently long period of time. A uniform current density is distributed in a circular region with $r \le r_0$. As to the gas density, we enhance it inside the magnetic island in order to model a dense filament material. Accordingly, the density at the center of the magnetic island is about 70 times larger than outside it, that is, $\rho = 1 + 2/\beta(1 - 4r^2)$ for $r \le r_0$ and $\rho = 1$ for $r > r_0$, where ρ is the dimensionless density and $\beta = 0.03$ is the plasma beta. In addition, the temperature is uniformly distributed (dimensionless temperature $T = 1$), and the specific heat ratio γ is set to be 5/3. The units of length, velocity, and time are $L_0 = 2 \times 10^4$ km, $v_A = 1050$ km s^{-1}, and $t_0 = L_0/v_A \sim 20$ s, where v_A is the Alfvén velocity measured just at the boundary of the magnetic island (at $r = r_0$). We also adopt typical coronal values as units of temperature and density, namely, $T_0 = 10^6$ K and $n_0 = 10^9$ cm^{-3}. The initial perturbation is made by adding an artificial force near the center of the magnetic island, that is, $F/\rho = -0.2 \exp(-\Psi)\ \mathrm{sgn}\ (v_c - 0.14 v_A)$, where F is a dimensionless volume force, "sgn" is the sign function, and v_c is the dimensionless velocity of the center of the magnetic island. In this simulation, the volume force makes the magnetic island start rising and keep its velocity around 0.14 v_A (150 km s^{-1}) after it is accelerated to this value. The resistivity $\eta = 0.02 \cos(6x) \cos[6(y - h_x)]$ is imposed in a local area of $|x| \le 0.26$ and $|y - h_x| \le 0.26$, where η is the dimensionless resistivity and h_x traces the location of an x-point below the magnetic island as it rises. The simulation is performed within the region of $0 \le x \le 8$, $0 \le y \le 16$ under the assumption of a symmetry with respect to the y-axis. We have 61 × 181 grids, which are distributed uniformly in the y-axis and nonuniformly in the x-axis, similar to Chen et al. (1999). The top ($y = 16$) and side ($x = 8$) boundaries are both free, and the bottom boundary ($y = 0$) is rigid with a line-tying effect.

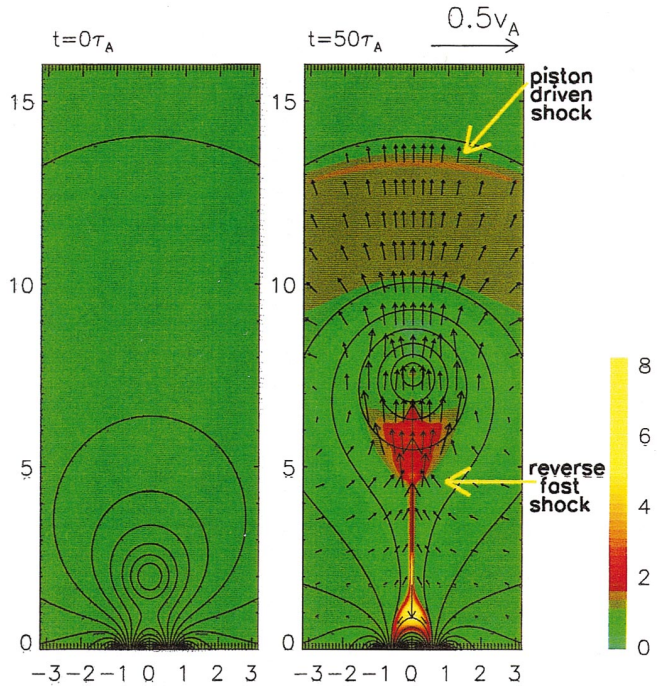

FIG. 1.—Evolution of plasmoid eruption. The contour lines represent magnetic field lines, the black arrows represent the fluid velocity field, and the color map represents temperature. The yellow arrows show the positions of the piston-driven fast shock and the reverse fast shock.

3. RESULTS

Figure 1 shows the eruption of a magnetic island, which is initially accelerated by a upward force. Although this force is an artificial force in this simulation, several studies so far suggest that a magnetic island rises under a net upward force in some environments (Forbes 1990; Chen 1996; Wu, Guo, & Dryer 1997; Gibson & Low 1998). After the magnetic island rises, it stretches the magnetic field lines, and a current sheet forms below it. Those gases around this sheet flow toward an x-point in the sheet, causing the fast-magnetic reconnection there because the resistivity is locally enhanced around this point (Magara & Shibata 1999). The resultant reconnection jets, one of which flows upward to collide with the bottom of the magnetic island and the other of which flows downward to collide with the top of a magnetic arcade, produce fast-mode MHD shocks in both cases (see the right panel in Fig. 1). Moreover, we also have a piston-driven fast shock in front of the ejecting magnetic island. All of these shocks can be seen clearly in Figure 2, indicating how the vertical component of fluid velocity is distributed along the y-axis at $t = 30$ and $t = 50$. Those fast shocks formed at the bottom, and in the front of the magnetic island, they move upward. Strictly speaking, the front shock is a forward shock, while the bottom shock is a reverse shock traveling downward, although the upward reconnection jet is so fast that the wave front of this shock apparently moves upward. Figure 3 displays the time variations of the heights of these two kinds of fast shocks as well as the center of the magnetic island. From this figure, we find that the front shock moves upward at a high speed ($0.2 v_A$) and that

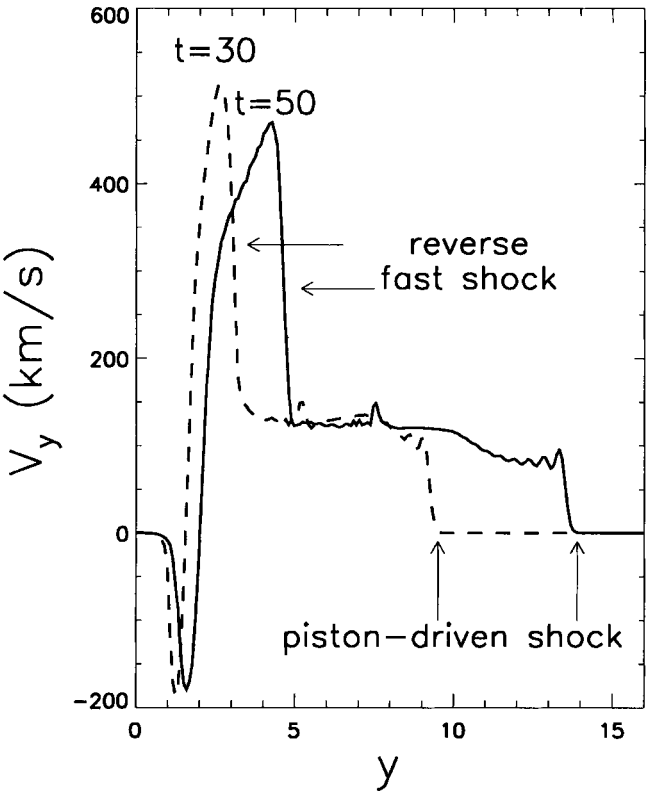

FIG. 2.—Spatial distributions of the vertical component of fluid velocity along the *y*-axis (symmetric axis). The dahsed line (time = 30) and the solid line (time = 50) are shown. The positions of piston-driven fast shock and the reverse fast shock are indicated by arrows.

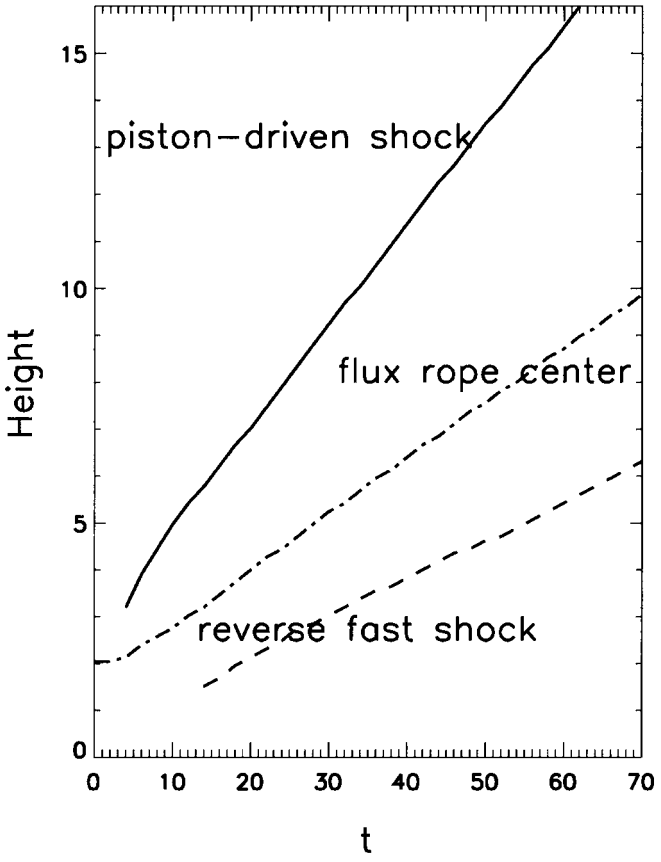

FIG. 3.—Height-time relations of piston-driven fast shock (*solid line*), flux rope center (*dot-dashed line*), and reverse fast shock (*dashed line*). The time variation of the flux rope center represents the motion of a filament material inside the rope.

the bottom shock rises rather slowly ($0.09v_A$), so that the interval between these two shocks becomes large with time.

4. DISCUSSION

Let us now introduce the main result of Reiner et al. (2000) about traveling radio sources. Figure 4 reproduces their original height-time data in a simplified manner to show readers the essence of their result. This figure has three kinds of height-time data, that is, the white-light CME data, the longer wavelength radio data (from the decametric to hectometric range), and the shorter wavelength radio data (the metric range). First, we would like to focus attention on the decametric-hectometric radio data. Their height-time relation is fairly coincident with that of the leading edge of the white-light CME data, which supports the well-established idea that decametric-hectometric type II bursts originate from the piston-driven fast shock that is formed in front of an eruptive plasmoid, where the shock enhances the gas density so that it appears bright in white light. In addition, the radio source of decametric-hectometric type II bursts travels from the upper corona to interplanetary space. These features are basically confirmed in our model. Figure 1 shows that a piston-driven fast shock is formed in front of an ejecting magnetic island, and Figure 2 shows that this shock is traveling outward. We then discuss metric type II bursts, the generator of which is rather unclear compared to decametric-hectometric type II bursts. Figure 4 gives us two important properties of metric type II bursts. One is that the source of metric type II bursts appears earlier and occupies lower positions (until its disappearance) than the source of decametric-

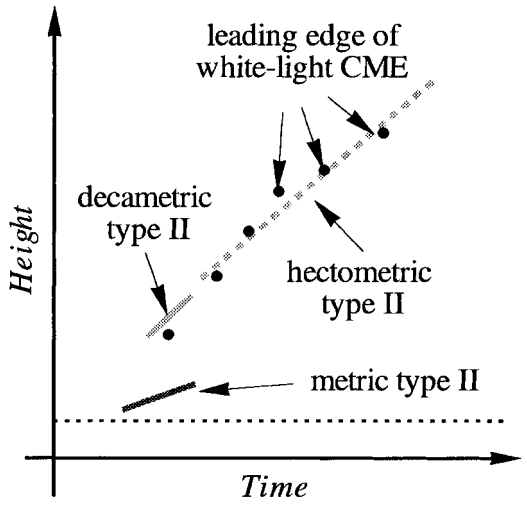

FIG. 4.—Height-time data of white-light CME (*points*), decametric (*light-gray solid line*), hectometric (*light-gray dotted line*), and metric (*dark-gray solid line*) type II radio bursts. The dotted horizontal line represents the level of the solar surface. This figure originated from Fig. 2 in Reiner et al. (2000) but is displayed in a simplified manner.

hectometric type II bursts. The other is that the source of metric type II bursts travels in the corona more slowly than the source of decametric-hectometric type II bursts and disappears in a short time. Our model can explain these two properties in the following way: The simultaneous existence of two radio sources at different positions means that they have distinct spatial origins in their formations, which is consistent with our result that the source of metric type II bursts is located in the fast shock that is formed at the bottom of the magnetic island, whereas the other source has its origin in the piston-driven fast shock formed in front of the same magnetic island. The speed and lifetime of the radio sources depend directly on the properties of the fast shocks in our model. The piston-driven fast shock that produces decametric-hectometric type II bursts is the forward shock traveling in a free space, while the shock-producing metric type II bursts are the reverse shock formed through the collision of a high-speed reconnection jet to "the wall of magnetic field." The reason why this reverse shock apparently moves upward is that the reconnection jet is so strong that it can move the magnetic wall upward, which implies that this reverse shock no longer goes upward and that it finally disappears when the energy released by the reconnection stops or weakens to reduce the speed of reconnection jet. Accordingly, our model suggests that the shock-producing decametric-hectometric type II bursts can travel in interplanetary space freely for a long time, whereas the shock-producing metric type II bursts travel in the corona at the same velocity as the magnetic wall (possibly slower than the former shock; see Fig. 3) for a short time while the strong reconnection jet is provided.

In summary, this is the first Letter to apply a phenomenological model, the so-called CSHKP model, to understand two kinds of shocks systematically. This model describes the physical processes of plasmoid eruption (Shibata 1996), and, as far as the coronal shock-producing metric type II bursts are concerned, we strongly suggest that the essence of their formation is directly connected to the occurrence of a strong reconnection jet below an eruptive plasmoid. From this viewpoint, detailed studies on the shock formation around the bottom of a plasmoid in more realistic environments will be needed in order to explain more precisely the properties of metric type II bursts and their related phenomena (Klassen et al. 2000). In our present study, we assume that an artificial force lifts the magnetic island, and we find that the reverse shock formed at the bottom of the magnetic island seems to survive for a long time because the magnetic reconnection remains effective through all of the simulation. These imperfect points will be improved in our following studies, in which such realistic components as the gravitational force, time-dependent resistivity, and three-dimensional effects are taken into consideration.

REFERENCES

Carmichael, H. 1964, in AAS-NASA Symp. on Solar Flares, ed. W. N. Hess (NASA SP-50; Washington, DC: NASA), 451
Chen, J. 1996, J. Geophys. Res., 101, 27499
Chen, P. F., Fang, C., Tang, Y. H., & Ding, M. D. 1999, ApJ, 513, 516
Cliver, E. W., Webb, D. F., & Howard, R. A. 1999, Sol. Phys., 187, 89
Feynman, J., & Hundhausen, J. 1994, J. Geophys. Res., 99, 8451
Feynman, J., & Martin, S. F. 1995, J. Geophys. Res., 100, 3355
Forbes, T. G. 1990, J. Geophys. Res., 95, 11919
Gibson, S. E., & Low, B. C. 1998, ApJ, 493, 460
Gopalswamy, N., & Kundu, M. R. 1992, in AIP Conf. Proc. 264, Particle Acceleration in Cosmic Plasmas, ed. G. P. Zank & T. K. Gaisser (New York: AIP), 257
Gosling, J. T., Hilder, E., MacQueen, R. M., Munro, R. H., Poland, A. I., & Ross, C. L. 1976, Sol. Phys., 48, 389
Hirayama, T. 1974, Sol. Phys., 34, 323
Hu, Y. Q. 1989, J. Comput. Phys., 84, 441
Hundhausen, A. J. 1999, in The Many Faces of the Sun, ed. K. T. Strong et al. (New York: Springer), 143
Kahler, S. W., Cliver, E. W., Sheeley, N. R., Jr., Howard, R. A., Koomen, M. J., & Michels, D. J. 1985, J. Geophys. Res., 90, 177
Klassen, A., Aurass, H., Mann, G., & Thompson, B. J. 2000, A&AS, 141, 357
Kopp, R. A., & Pneuman, G. W. 1976, Sol. Phys., 50, 85
Low, B. C. 1996, Sol. Phys., 167, 217
Low, B. C., Munro, R. H., & Fisher, R. R. 1982, ApJ, 254, 335
Magara, T., & Shibata, K. 1999, ApJ, 514, 456
Priest, E. R. 1988, ApJ, 328, 848
Reiner, M. J., Kaiser, M. L., Plunkett, S. P., Prestage, N. P., & Manning, R. 2000, ApJ, 529, L53
Rust, D. M., & Kumar, A. 1996, ApJ, 464, L199
Shibata, K. 1996, Adv. Space Res., 17, 9
Steele, C. D. C., & Priest, E. R. 1989, Sol. Phys., 119, 157
Sturrock, P. A. 1966, Nature, 211, 695
Wu, S. T., Guo, W. P., & Dryer, M. 1997, Sol. Phys., 170, 265